ACS APPLIED MATERIALS & INTERFACES

Research Article

www.acsami.org

Facile Fabrication of Biocompatible and Tunable Multifunctional Nanomaterials via Iron-Mediated Atom Transfer Radical Polymerization with Activators Generated by Electron Transfer

Weiwei He,[†] Liang Cheng,[‡] Lifen Zhang,[†] Zhuang Liu,*[,‡] Zhenping Cheng,*[,†] and Xiulin Zhu*[,†]

[†]Jiangsu Key Laboratory of Advanced Functional Polymer Design and Application, Department of Polymer Science and Engineering, College of Chemistry, Chemical Engineering and Materials Science, Soochow University, Suzhou, Jiangsu 215123, China

[‡]Institute of Functional Nano & Soft Materials (FUNSOM) and Jiangsu Key Laboratory for Carbon-Based Functional Materials and Devices, Soochow University, Suzhou, Jiangsu215123, China

Supporting Information

ABSTRACT: A novel strategy of preparing multifunctional nanoparticles (NPs) with near infra red (NIR) fluorescence and magnetism showing good hydrophilicity and low toxicity was developed via surface-initiated atom transfer radical polymerization with activators generated by electron transfer (AGET ATRP) of poly(ethylene glycol) monomethyl ether methacrylate (PEGMA) and glycidyl methacrylate (GMA) employing biocompatible iron as the catalyst on the surface of silica coated iron oxide (Fe_3O_4@SiO_2) NPs. The small molecules (CS2), a NIR fluorescent chromophore, can be fixed into the covalently grafted polymer shell of the NPs by chemical reaction through a covalent bond to obtain stable CS2 dotted NPs Fe_3O_4@SiO_2@PPEGMA-*co*-PGMA@CS2. The fluorescence intensity of the as-prepared NPs could be conveniently regulated by altering the silica shell thickness (varying the feed of silica source TEOS), CS2 feed, or the feed ratio of V_{PEGMA}/V_{GMA}, which are easily realized in the preparation process. Thorough investigation of the properties of the final NPs including *in vivo* dual modal imaging indicate that such NPs are one of the competitive candidates as imaging agents proving a promising potential in the biomedical area.

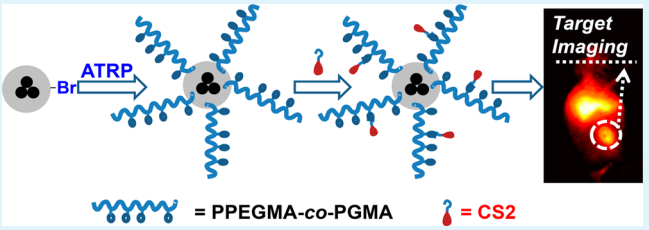

KEYWORDS: *AGET ATRP, iron catalyst, NIR, magnetism, nanoparticles, in vivo*

INTRODUCTION

Multifunctional nanoparticles (NPs) with magnetism and fluorescence have received wide attention recently because of their promising potential as dual modal contrast agents in the biomedical area combining advantages of high spatial resolution of magnetic resonance imaging (MRI) and high intensity of fluorescence; the past decade witnessed its rapid development: preparation and investigation of the potential in biomedical application.[1−9] Up to now, although several methods and varying structures of such promising NPs have been developed,[10] synthesis of these NPs with optimum and satisfying characteristics suitable for application including in vivo detection as well as other biorelated utilization is still a big challenge. As demonstrated by previous documents, contact with the magnetic iron oxide may cause photoquenching of the fluorophore largely decreasing the intensity, thereby exhibiting a low sensitivity, an important index for imaging. To solve such a shortcoming, a core-shell structure consisting of the magnetic iron oxide core and a protecting shell isolating the luminescence source from the magnetic core is generally adopted when preparing such NPs. Silica is a popular material as the protecting shell[11−13] offering several advantages: 1) silica is physically inert with rare or slight effects to the internal properties of the functionalities of different parts; 2) it is optically transparent; 3) it could improve the hydrophilicity and biocompatibility of the NPs; 4) numbers of hydroxyl groups on the surface make it quite convenient to modify with other functional groups or attach biomolecules. Besides, the process of introducing the silica shell is relatively simple and well developed.

In most of the reported cases of multifunctional NPs with magnetism and fluorescence, the fluorophore emit light in the UV-vis range,[5−9] and barriers emerge when employing such materials in vivo caused by high light scattering, autofluorescence, and high absorption of the tissues in the body, except that the UV light also might cause damage to the body; all of these restrict the application of such materials. Luckily, all of the compounds in the body show their lowest absorption coefficients in the near infrared (NIR, 650−900 nm) range allowing access to deeper penetration into the tissue; besides low or no background fluorescence generates in the NIR range, these unique characters of NIR fluorophore attract wide attention, and various materials capable of emitting NIR light have been proposed including quantum dots (QDs),[14−17]

Received: July 7, 2013
Accepted: September 13, 2013
Published: September 30, 2013

lanthanides compounds,[18,19] upconversion materials,[20−22] and organic dyes (including polymers).[23−29]

To date some reports about preparation of multifunctional NPs with magnetism and NIR fluorescence have been demonstrated;[30,31] however, most of them were based on heavy metals, e.g. lanthanide[12,32,33] and QDs,[34,35] which are quite toxic, and safety concerns will come up when employing these materials in the biological area. In the cases of much less toxic organic dyes, most of the proposed materials are built on physical interaction between magnetic and fluorescent functionalities,[9,36,37] and few reports using dyes emitting light in the range of 650−700 nm by a short linkage between them were also proposed;[38,39] unfortunately excitation in visible light range might restrict its application in biology because of its low penetration in the tissue.

The toxicity of these synthesized NPs was much less investigated and rare systemic investigation was made but a few individual cases declaring biocompatibility of the as-prepared NPs under specific conditions. To now, it is still unclear whether the synthetic NPs are safe when performing in vivo administration. Anyway, it is publicly considered that the surface property plays a critically important role in its toxicity of the integrity by adjusting the hydrophilicity and dispersibility of the NPs.[40] Hydrophilicity is thought to be one of the prerequisites for a qualified in vivo imaging agent, which is often achieved by an optimum surface modification. To achieve this, small molecules, such as ligands, as well as polymers are usually employed.[41−44] Small molecules and the physically polymer decorated NPs often suffer a stability issue because ligand exchange is prone to occur in an available condition during the process of either preparation or application. Covalent binding of the polymers to the NPs by "grafting to" or "grafting from" makes the NPs much more stable and viewed as the mainly used technique. The nearly fully developed living radical polymerization techniques render such a process much more convenient offering densely uniform polymers chains on the surface. Among them, ATRP is the most used and best investigated one,[45−50] since it is quite convenient to introduce initiators to the surface of NPs.[51−54]

Herein we report a novel strategy of preparing stable NPs consisting of organic dyes with both excitation and emission in NIR range and magnetic iron oxide showing good hydrophilicity and excellent biocompatibility via surface-initiated activators generated by electron transfer ATRP (SI-AGET ATRP) of poly(ethylene glycol) monomethyl ether methacrylate (PEGMA) and glycidyl methacrylate (GMA) employing biocompatible iron as the catalyst on the surface of silica coated iron oxide NPs; the fluorophore CS2 was embedded into the polymer matrix by a covalent bond as shown in Figure 1a. It is well known that AGET ATRP combines both advantages of normal and reverse ATRP. In this process, a much more stable transition metal with a high oxidation state and a reducing agent were used to generate an active catalyst with a low oxidation state, which facilitates to conduct the synthetic procedures easily.[53] The amount of CS2 in the NPs as a result of the optical properties of the NPs could be facilely adjusted by changing the CS2 feed and the active sites (GMA segments of the copolymer chain) of the copolymer shell. In addition, altering the silica source feed could have an effect on the structure of the core-shell NPs therefore also showing an effect toward the optical properties of the final materials. CS2 molecules were fixed into the copolymer shell by covalent bonds; hence the materials show good stability. The potential of the as-prepared NPs as a dual modal contrast agent in vivo imaging was investigated.

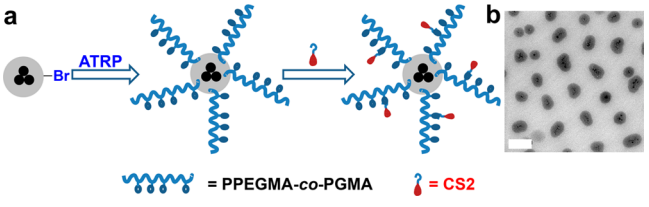

Figure 1. (a) Synthetic route to prepare multifunctional NPs via AGET ATRP mediated by iron catalyst and (b) TEM image of the as-prepared NPs. Scale bar = 50 nm.

EXPERIMENTAL SECTION

Materials. PEGMA (M_n = 475 g/mol (denoted as $PEGMA_{475}$) and 1100 g/mol (denoted as $PEGMA_{1100}$), >99%) were purchased from Aldrich; they were purified by passing through a column filled with neutral aluminum oxide and stored at −18 °C before use. GMA was purchased from Shanghai Chemical Reagents Co. (Shanghai, China) and was purified by distillation under reduced pressure. Ferric acetylacetonate (97%), 1,2-dodecanediol (90%), oleic acid (90%), oleic amine (70%), benzyl ether (99%), ammonia ($NH_3.H_2O$, 28%), 3-aminopropyl triethoxysilane (APTES, 99.0%), and dopamine hydrochloride (95%) were purchased from Aldrich and were used as received. Triton X-100 was purchased from J&K and was used as received. Tetraethoxysiliane (TEOS, >98%, Fluka) was used as received. Ascorbic acid (AsAc, >99.7%) and 2-bromoisobutyryl bromide (BiBB, 98%) were purchased from Shanghai Chemical Reagents Co. (Shanghai, China) and were used as received. Triethylamine (TEA, AR) and *N*,*N*-dimethyl formamide (DMF, AR) were obtained from Shanghai Chemical Reagents Co. (Shanghai, China) and dried with activated molecular sieves (4 Å). Toluene (AR) was purchased from Shanghai Chemical Reagents Co. (Shanghai, China) and was dried by distillation with sodium. Ferric chloride hexahydrate ($FeCl_3{\cdot}6H_2O$) (>99%), tetrahydrofuran (THF, AR), ethanol (AR), hexanol (AR), cyclohexane (AR), and all other chemicals were obtained from Shanghai Chemical Reagents Co. (Shanghai, China) and were used as received unless mentioned.

Synthesis of ATRP Initiator-Immobilized NPs (Fe_3O_4@SiO_2−Br). The colloidal magnetic iron oxide NPs with an average size of 6 nm were prepared according to ref 55. The NPs were modified to be hydrophilic by ligand exchange with dopamine. Silica shell was coated by hydrolysis of TEOS according to an inverse emulsion method.[56] APTES was used to introduce amine groups on the surface of NPs to get Fe_3O_4@SiO_2−NH_2 NPs, which was reacted further with BiBB to obtain Fe_3O_4@SiO_2−Br. Generally, ∼3 mg of Fe_3O_4 NPs was added to a reverse emulsion of hexanol (32.0 mL), triton X-100 (34.0 mL), cyclohexane (150.0 mL), water (12.0 mL), and ammonium water (2.5 mL). After having been stirred for 2 h, 0.6 mL of TEOS was added; reacting 24 h, 0.1 mL of APTES was added, and the amine modified NPs were collected and washed by centrifugation after another 16 h. The obtained NPs were added to 50 mL of THF; 0.3 mL of TEA was added, and then the suspension was put into an ice water bath. A mixture of 0.3 mL of BiBB in 5 mL of THF was added dropwise, and the NPs were collected and washed by centrifugation after 6 h.

General Procedure for SI-AGET ATRP of PEGMA and GMA from Fe_3O_4@SiO_2−Br. A typical polymerization procedure was as follows: $FeCl_3{\cdot}6H_2O$ (0.49 mg, 3.6 μmol), TDA-1 (17.4 μL, 10.8 μmol), Fe_3O_4@SiO_2−Br (30 mg), AsAc (3.2 mg, 3.6 μmol), $PEGMA_{475}$ (0.8 mL, 1.8 mmol), GMA (0.2 mL, 1.5 mmol), and DMF (2.0 mL) were added to a dried ampoule to give a well-dispersed suspension under stirring and treated in ultrasonic for 5 min. After bubbling for 5 min with Ar, the ampoule was flame-sealed and transferred into an oil bath held by a thermostat at the desired temperature (90 °C) to polymerize under vigorous stirring. After the desired polymerization time, the ampoule was cooled by immersing it

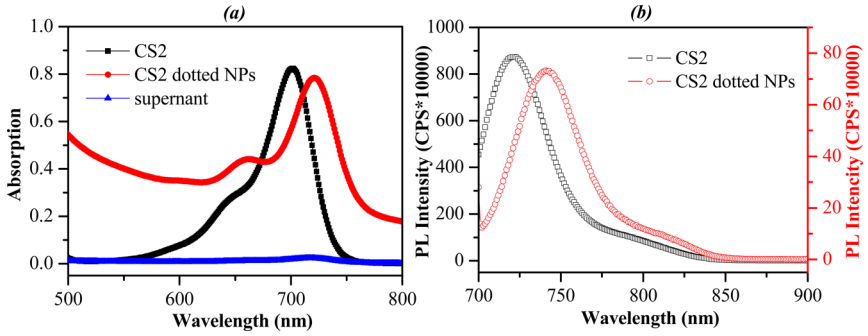

Figure 2. (a) UV/vis/NIR and (b) fluorescence spectra of CS2, CS2 dotted NPs in ethanol. Ex = 690 nm.

into iced water, the NPs were washed with abundant THF and acetone in ultrasonic and collected by centrifugation and repeated several times.

Preparation of CS2 Dotted NPs: Fe_3O_4@SiO_2@PPEGMA-co-PGMA@CS2. Typically, 3.0 mg of CS2 (synthesized according to ref 26) and 1.0 mg of TBABr were added to the dispersion of Fe_3O_4@SiO_2@PPEGMA-co-PGMA NPs in acetonitrile. The mixture was heated and refluxed under stirring and protection of Ar. After 6 h, the CS2 dotted NPs were collected and washed by repetition of sonication and centrifugation alternatively.

Culture of HeLa Cells and Confocal Laser Scanning Microscopy. HeLa cells were cultured in Dulbecco's modified eagle medium (DMEM) containing 10% fetal bovine serum (FBS), streptomycin (100 U mL^{-1}), penicillin (100 U mL^{-1}), and 4 mM L-glutamine at 37 °C in a humidified 5% CO_2-containing atmosphere. Human embryonic kidney 293T cells were cultured in Dulbecco's modified eagle medium (DMEM) containing 10% FBS and 1% penicillin/streptomycin at 37 °C in a humidified 5% CO_2-containing atmosphere.

Fluorescence images of cells were taken by a laser scanning confocal fluorescence microscope (TCS SP5 Leica). An excitation wavelength of 488 nm was chosen for the fluorescence imaging of Hela cells and 633 nm for CS2 dotted NPs.

Cytotoxicity Assay by MTT. The MTT assay was performed to evaluate the impact of CS2 dotted NPs on the viability of Hela and 293T cells. The cells were seeded onto 96-well plates at a density of 1 × 10^4 cells/well for 24 h. Afterwards a series of concentrations of CS2 dotted NPs were added into the cell culture. After 24 h incubation, 20 mL of MTT solution in phosphate buffered saline (PBS) was added to each well and incubated for an additional 4 h. The cell culture was discarded afterwards with 150 mL of dimethyl sulfoxide (DMSO) added to each well. We then incubated the plate at 37 °C for 5 min and shocked it for another 10 min at room temperature to allow for the complete dissolving of formazan. Finally, the absorbance at 570 nm of each well was measured by a microplate reader (Model 680 Bio-RAD) to determine the relative cell viability.

In Vivo Fluorescence/MR Dual-Modal Imaging. Female nude and Kunming mice were obtained from Suzhou Belda Bio-Pharmaceutical Co. and used under protocols approved by Soochow University Laboratory Animal Center. To develop KB tumors, 5 × 10^6 KB cells suspended in serum-free cell medium were injected on the shoulder of each nude mouse. After ~2 weeks, tumor-bearing mice were injected with CS2 dotted NPs (200 μL, 2 mg/mL based on iron element) for in vivo imaging. In vivo fluorescence imaging was carried out using NIR (704 nm) as the excited wavelength, and light between 750−900 nm was collected. MR imaging studies were conducted on a 3-T clinical MRI scanner (Bruker Biospin Corporation, Billerica, MA, USA) equipped with a special coil designed for small animal imaging.

Measurements. Fourier transform infrared (FT-IR) spectra were recorded on a NICOLET-6700 FTIR spectrometer. Thermogravimetric analysis (TGA) was carried out on a 2960 SDT TA Instruments with a heating rate of 10 °C/min from the room temperature to 800 °C under the nitrogen atmosphere. Transmission electron micrographs were taken with a FEI TecnaiG220 (TEM) operated at an accelerating voltage of 200 kV. XRD (PANalytical Company, X'PERT PRO MPD, Cu Ka, l = 1.5406 Å, X' Celerator) was used to determine the crystal structure of the pristine magnetic NPs. Fluorescent emission spectra were measured with excitation light of 294 nm in a PerkinElmer Ls-50B. A vibrating-sample magnetometer (VSM-7407, LakeShore, USA) was used at room temperature to measure the magnetic properties of Fe_3O_4 and magnetic composite particles. Fe elemental analysis was made by inductively coupled plasma (ICP) of Vista MPX. The number-average molecular weight (M_n) and molecular weight distribution (M_w/M_n) values of the resultant polymers were determined using a Waters 1515 gel permeation chromatograph (GPC) equipped with a refractive-index detector (Waters 2414), using HR 1 (pore size: 100 Å, 100−5000 Da), HR 2 (pore size: 500 Å, 500−20 000 Da), and HR 4 (pore size 10 000 Å, 50−100 000 Da) columns (7.8 × 300 mm, 5 μm beads size) with measurable molecular weights ranging from 10^2 to 5 × 10^5 g/mol. THF was used as the eluent at a flow rate of 1.0 mL/min and 40 °C. GPC samples were injected using a Waters 717 plus autosampler and calibrated with poly(methyl methacrylate) standards purchased from Waters. The sizes of nanoparticles were measured using ZEN3690 zetasizer (Malvern, USA).

RESULTS AND DISCUSSION

Preparation of CS2 Dotted NPs. The route to prepare CS2 dotted NPs is illustrated in Figure 1a. The synthetic route to prepare Fe_3O_4@SiO_2−Br is shown in Scheme S1, its preparation and further SI-AGET ATRP are verified by various techniques including TEM, DLS, FT-IR, XPS, XRD, and TGA (Figures S1−S6). After decoration with polymers, the Fe_3O_4@SiO_2@PPEGMA-*co*-PGMA NPs show good dispersion (Figure 1b). The grafted copolymers were etched using HF from the silica coated iron oxide in THF and were collected. Copolymers (M_n = 20900 g/mol, M_w/M_n = 1.39) were obtained by precipitating in hexane and dried in vacuum.

Silica shell coating is an important step in determining the final performance of the as-prepared NPs in application; the silica shell not only acts as the protective layer (isolating of the core material from outside environment for keeping core material stable and suppressing the photoquenching effect of the magnetic iron oxide to the fluorophore) but also serves as substrate for further modification with polymers employing the AGET ATRP technique. The silica shell thickness could facilely be modulated by adding a varying dose of precursor TEOS. In this work NPs of average 22, 16, and 10 nm thickness of silica shell were fabricated by adding 600, 400, and 200 μL of TEOS respectively as shown in Figure S1b−d. ATRP was chosen to modify the surface of the silica coated NPs as it is quite convenient and mature to introduce the ATRP initiator on the surface of the material, and the composition of the grafted copolymer could be facilely regulated by varying the feed ratio of the monomers. However, a transition metal should be added as the catalyst, which might have a negative effect on the quality

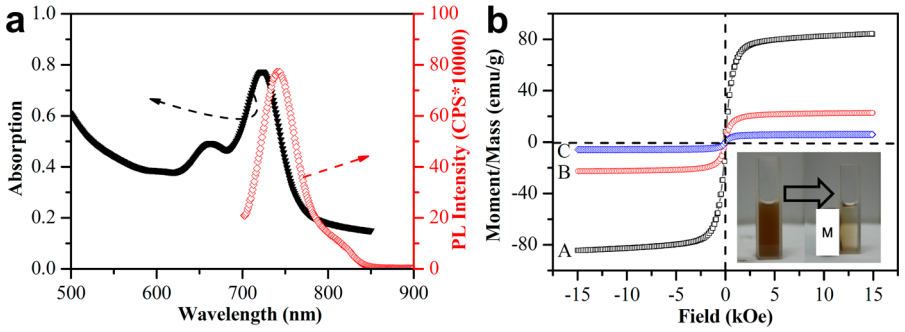

Figure 3. (a) UV/vis/NIR and fluorescence spectra of CS2 dotted NPs in water, iron concentrations is 0.3 mg/mL, ex = 690 nm; CS2 feed: 3 mg. (b) Magnetic hysteresis loops at 300 K for the obtained NPs of (A) Fe_3O_4, (B) Fe_3O_4@SiO_2, and (C) $Fe_3O_4$00@SiO_2@PPEGMA$_{475}$-*co*-PGMA@CS2; inset is a photo of the as-prepared NPs dispersed in water before and after administration of a external magnetic field, M represents magnetic bar.

of the final materials. Hence, in this case iron-mediated AGET ATRP was employed to adjust the surface properties of the NPs because of its easy operation, available raw materials, and convenient immobilization of initiator on silica surface and biocompatible iron catalyst was elaborately chosen to avoid/decrease interference of the residual transition metal catalyst in further bioapplication. The physical property of the surface can be readily modified by choosing various monomers. In this work, we chose PEGMA and GMA to copolymerize for three reasons: firstly, a certain length of polymer chains could further minimize the quenching effect of the magnetic core on the CS2; secondly PEGMA is hydrophilic that helps improving the colloids stability of the NPs in water; lastly, GMA, which bearing an epoxy group, provides active sites to fulfill the immobilization of the carboxylic group bearing the CS2 dye into the NPs as shown in Figure 1a.

CS2 can be readily fixed on Fe_3O_4@SiO_2@PPEGMA-*co*-PGMA NPs by a chemical reaction between the carboxyl groups of CS2 and epoxide groups of PGMA segment of the copolymer chains to obtain the CS2 dotted NPs Fe_3O_4@SiO_2@PPEGMA-*co*-PGMA@CS2. This is verified by UV-vis-NIR and fluorescence means. In Figure 2a, CS2 dotted NPs show a red shift relative to the free dye (with absorption peak at 700 nm) and has a maximum absorption at 720 nm in ethanol; meanwhile when separated by magnetic separation, the supernatant shows nearly no absorption indicating successful linking of the dye to the NPs. The fluorescence of CS2 dotted NPs in ethanol also exhibited a red shift (from 721 to 741 nm) comparing to free CS2 (Figure 2b); besides, the intensity of NPs suspension is lower than the that of free dye probably caused by a synergetic effect of the photoquenching of the magnetic core and mutual quenching of the dyes embedded in the polymer matrix.

Optical and Magnetic Properties. The optical properties of CS2 dotted NPs in water (Figure 3a) are similar to that in ethanol exhibiting almost the same fluorescence intensity also indicating good dispersibility of the as-prepared NPs in water. NPs with a thick shell (22 nm) resulted in higher intensities (772, 000 CPS) as expected because of the effective protection of thick silica shell from photoquenching of the iron oxide core.

The magnetic properties of the Fe_3O_4, Fe_3O_4@SiO_2, and Fe_3O_4@SiO_2@PPEGMA$_{475}$-*co*-PGMA@CS2 NPs were recorded using a VSM with fields up to 15000 Oe. As shown in Figure 3b, hysteresis loops of the samples were registered at 300 K. Silica coated magnetic NPs reach a saturation moment of 22.6 emu g^{-1}. This saturation magnetization value is lower than the saturation magnetization of the bare Fe_3O_4 NPs (84.0 emu g^{-1}) because of the diamagnetic contribution of the thick silica shell surrounding the magnetic cores. Similarly, the saturation magnetization value of the Fe_3O_4@SiO_2@PPEGMA$_{475}$-*co*-PGMA@CS2 NPs decreased to 5.9 emu g^{-1}, which is much lower than the Fe_3O_4 NPs as well as the silica coated ones for the same reason indicating further wrapping with a polymer shell which is consistent with the outcomes of TEM and TGA analysis (seen in the Supporting Information). Neither coercivity nor remanence is observed among the three magnetization curves, indicating the superparamagnetic behavior of the as-prepared NPs at 300 K. Due to the screening effect of the silica and copolymer layers, the Fe_3O_4@SiO_2@PPEGMA$_{475}$-*co*- PGMA@CS2 NPs can be readily and stably dispersed in water (inset of Figure 3b); however, when subjected to a strong external magnetic field the NPs can be removed from the solvent, indicating the NPs still remain good magnetism after a series of surface modification.

It is quite interesting that the fluorescence intensity of the as-prepared NPs could be conveniently regulated by altering the silica shell thickness (varying the feed of silica source TEOS), CS2 feed, or the value of V_{PEGMA}/V_{GMA} which are easily realized in the preparation process. As Figure S1b–d shows, the numbers of the iron oxide core change as altering the TEOS feed, displaying different core-shell structures and different average silica shell thickness, which has an effect on the optical properties of the final materials. The fluorescence intensity of as-prepared NPs increases with increasing silica shell thickness; this is probably because thicker silica shell could better avoid the bleaching effect of magnetic core to the fluorophore (Figures 4a); higher CS2 feed or lower V_{PEGMA}/V_{GMA} feed ratio can also enhance the fluorescence intensity due to a high concentration of CS2 in NPs (Figures 4b and 4c).

Cell Viability and In Vitro Imaging. The cytotoxicity of the multicomponent NPs is critically important towards further in vivo application. To reduce the toxicity of the CS2 dotted NPs, we designed a specific route, namely immobilizing CS2 into the outside polymers grafted on the surface of the NPs which guarantee the hydrophobic CS2 well distributed in the NPs accordingly dispersed finely in an aqueous environment providing sufficient fluorescence intensity. The hydrophilic and biocompatible grafted polymers PPEGMA-*co*-PGMA grow directly from the surface of the NPs via iron-mediated AGET ATRP; here environmentally friendly iron salt was deliberately selected as the catalyst intending to get rid of toxicity brought in by an unavoidable residual transition metal catalyst. The CS2

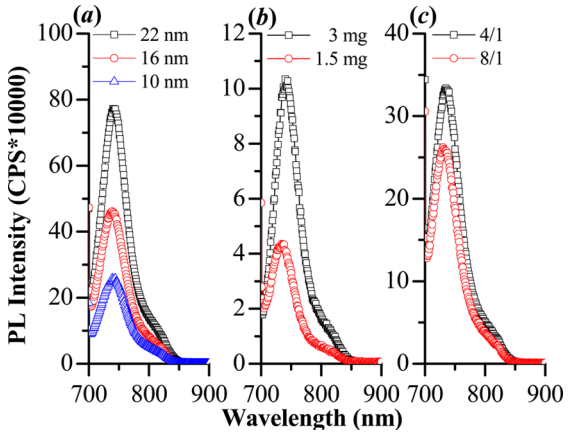

Figure 4. Effect of (a) silica shell thickness, (b) varying CS2 feed, and (c) altering the V_{PEGMA}/V_{GMA} feed ratio on fluorescence spectra of the as-prepared NPs in water. Ex = 690 nm.

dotted NPs are nontoxic with our elaborate design. Figure 5a shows the MTT assay of the CS2 dotted NPs incubated with HeLa cells; there are nearly no dead cells in the presence of NPs with iron concentrations less than 19 μg/mL, and even in high iron concentrations (600 and 300 μg/mL) there is still about 80% of the cell that survived. Cytotoxicity of the materials towards 293T cells was also investigated by MTT assay, and the results are illustrated in Figure S7. The results reveal that such materials of iron concentration of less than 50 μg/mL display biocompatibility towards 293T cells.

Then CS2 dotted NPs were incubated with HeLa cells for confocal fluorescence imaging. Under 633 nm laser excitations, a strong red fluorescence up to 700 nm (CS2) is observed indicating obvious colocalization. The NPs are spontaneously internalized into HeLa cells by endocytosis, and they are found in the cytoplasm of the HeLa cells but not in the nucleus (Figure 5b–d). Fluorescence imaging of HeLa cells incubated with different concentrations of CS2 NPs were studied as illustrated in Figure S8. It is found that more NPs entered into the cell membrane when increasing the materials concentration.

To validate the contrasting capacity of the hydrophilic Fe_3O_4@SiO_2@PPEGMA-*co*-PGMA@CS2 samples in contrasting MR images, MR images at 3.0 T on an Artoscan Imager, commonly used for clinical investigation of diseases in articulations, were collected. MR images of the sample with different concentrations (0, 55.8, 111.6, 223.2, and 446.4 μmol/L) were taken as shown in Figure 5e. The images become darker and darker with iron concentration increase, showing a transverse reflexivity (r_2) of 81.6 mM^{-1} s^{-1} (Figure 5f), which indicates an effective T_2 contrast agent of the as-prepared NPs.

In Vivo Imaging. The imaging ability of the CS2 dotted NPs is evidenced by in vivo imaging test in a mouse. After administrated for 5 h (Figure S9a), the signal of CS2 dotted NPs was detected all over the body and concentrated in a few areas because of accumulation of CS2 dotted NPs in specific organs in the mouse after 24 h as shown in Figure S9b. To further check the localization of the CS2 dotted NPs, the mouse was euthanized, and the main organs were subjected to fluorescence imaging. As shown in Figures S9c and 9d, CS2 dotted NPs were mainly localized in the spleen and liver.

The passive targeting capacity of CS2 dotted NPs in tumors is studied choosing KB tumors bearing a female mouse. After administrated in the body, the CS2 dotted NPs were detected by an in vivo imaging system, and the signals scatter all over the body (0.5, 2, and 4 h after administration in Figure 6a); however, after a long time (24 h), besides at the liver and spleen areas signals at the tumor spots are also more obvious than the other areas indicating good passive targeting capacity towards tumors of the as-prepared CS2 dotted NPs. Ex vivo images (Figure 6b) show similar outcomes. In vivo MR imaging further confirms the location and accumulation of CS2 dotted NPs in the tumors as shown in Figures 6c and 6d. The tumor area of the mouse after materials administration was a little darker than before, which is probably due to a low level of materials accumulated in the tumor area. T_2 signal intensity of the tumor areas reduced to 74% of that of the control one (Figure 6e). Moreover, the iron concentrations in tumors of the mice with and without materials administration were determined by the ICP technique, and ~1 mg/g concentration

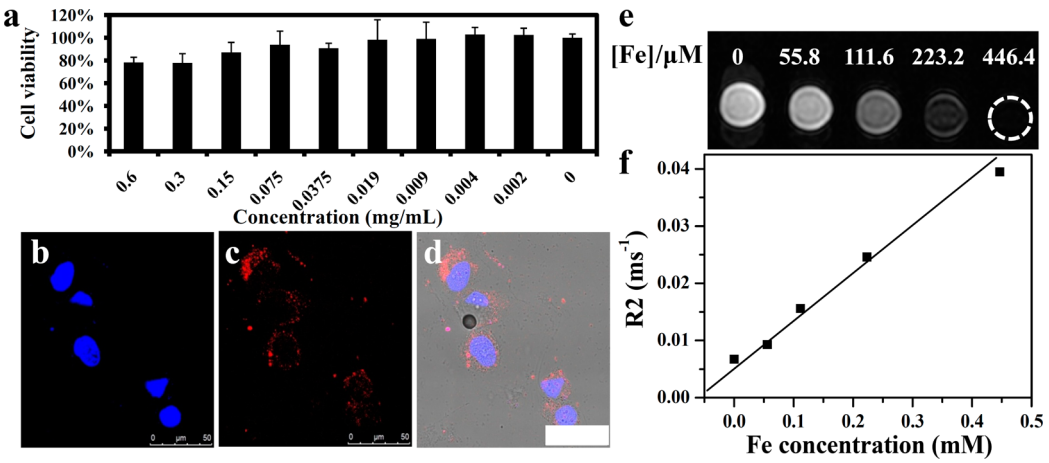

Figure 5. (a) Relative cell viability data of HeLa cells incubated with a series of iron concentrations of CS2 dotted NPs measured by the MTT cell viability assay; the incubation time was 24 h; error bars were based on triplicated samples. Confocal fluorescence images of CS2 dotted NPs transfected HeLa cells: (b) nucleus of HeLa cells, (c) CS2 dotted NPs, and (d) merged images, scale bar = 50 μm. (e) T_2-weighed MR images (3.0 T; TR, 2000.00 ms; TE, 12.9 ms) of the Fe_3O_4@-SiO_2@PPEGMA-*co*-PGMA@CS2 NPs. The iron concentration from left to right is 0, 55.8, 111.6, 223.2, and 446.4 mmol L^{-1}, respectively. (f) The T_2 relaxation rates (r_2) of Fe_3O_4@-SiO_2@PPEGMA-*co*-PGMA@CS2 NPs at different Fe concentrations.

dx.doi.org/10.1021/am402696p | ACS Appl. Mater. Interfaces 2013, 5, 9663–9669

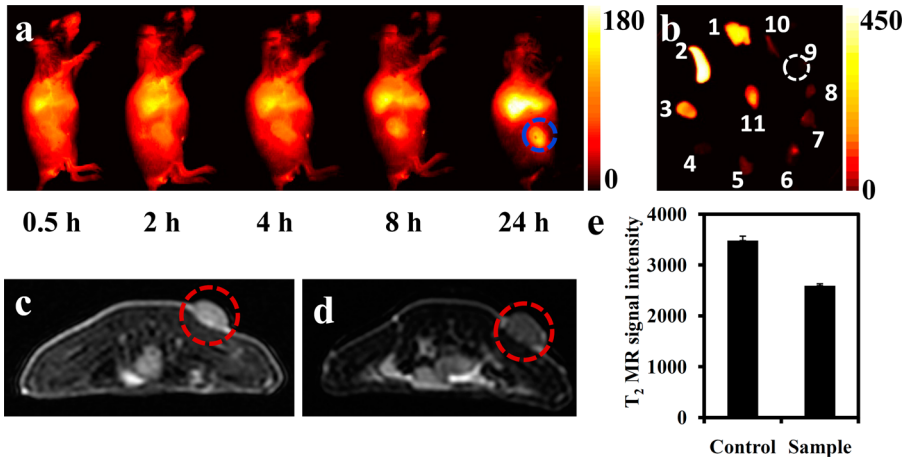

Figure 6. In vivo dual modal imaging of CS2 dotted NPs. In vivo NIR fluorescence images of KB tumor bearing Balb/c mouse at different time points post-injection of CS2 dotted NPs (a). Ex in vivo NIR image of mouse being administrated with CS2 dotted NPs after 24 h (b); excitation wavelength: 704 nm; images were obtained through a 760 nm filter: 1. liver, 2. spleen, 3. kidney, 4. heart, 5. lung, 6. stomach, 7. small intestine, 8. muscle, 9. bone, 10. skin, 11. tumor; the red cycle marks the tumor area. In vivo MR images of KB tumor bearing Balb/c mouse administrated with CS2 dotted NPs before (c) and after (d) NPs administration; the red circle marks the tumor areas. The corresponding T_2 signal values at the tumor areas (e).

enhancement was detected in the tumor of the mouse with materials administration, which indicates the accumulation of iron-based NPs in the tumor.

In addition, $PEGMA_{1100}$, instead of $PEGMA_{475}$ was used to copolymerize with GMA to graft on the surface of Fe_3O_4@SiO_2−Br NPs considering improving hydrophilicity of the NPs. The resulting CS2 dotted NPs show nearly the same fluorescence intensity at lower concentrations (Figure S10) and also reveal good passive targeting capacity at the tumor after 24 h of administration in the mouse (Figure S11).

CONCLUSIONS

In summary, an effective strategy to prepare hydrophilic bifunctional NPs with superparamagnetism and NIR fluorescence is developed successfully via SI-AGET ATRP employing a biocompatible iron catalyst. In this protocol an inverse emulsion method is adopted to prepare silica coated Fe_3O_4 NPs with high quality as the substrate which is further modified to be an ATRP initiator for further grafting hydrophilic and functional polymers. The NIR dye CS2 is immobilized into the polymer shell by a covalent bond taking advantage of the chemical reaction between active groups in grafted polymers and CS2. The final NPs are biocompatible according to MTT assay and dual modal in vivo imaging, namely fluorescence and MRI are successfully performed employing the as-prepared NPs as a contrast agent indicating good imaging property of the NPs; besides the NPs also reveal the capacity to target the tumors.

ASSOCIATED CONTENT

Supporting Information

TEM, DLS, FT-IR, XPS, XRD, and TGA analysis of the NPs at different levels; cytotoxicity of the materials towards 293T cells; imaging of different concentration of the prepared materials; biodistribution of the CS2 dotted NPs in mouse; optical and in vivo imaging of CS2 dotted NPs grafted by $PPEGMA_{1100}$-*co*-PGMA. This material is available free of charge via the Internet at http://pubs.acs.org.

AUTHOR INFORMATION

Corresponding Author

*Fax: +86-512-65882787. E-mail: chengzhenping@suda.edu.cn (Z.C.). E-mail: zliu@suda.edu.cn (Z.L.). Fax: +86-512-65112796. E-mail: xlzhu@suda.edu.cn (X.Z.).

Author Contributions

Weiwei He and Liang Cheng contributed equally to this work.

Notes

The authors declare no competing financial interest.

ACKNOWLEDGMENTS

The financial support from the National Natural Science Foundation of China (Nos. 21174096, 21274100, and 21234005), the Specialized Research Fund for the Doctoral Program of Higher Education (Nos. 20103201110005 and 20123201130001), the Project of International Cooperation of the Ministry of Science and Technology of China (No. 2011DFA50530), and the Project Funded by the Priority Academic Program Development of Jiangsu Higher Education Institutions (PAPD) is gratefully acknowledged. We thank Dr. Yonggang Li and Dr. Liang Guo from Department of Radiology at the First Affiliated Hospital of Soochow for their help in MR imaging.

REFERENCES

(1) Andolina, C. M.; Klemm, P. J.; Floyd, W. C.; Fréchet, J. M. J.; Raymond, K. N. *Macromolecules* **2012**, *45*, 8982−8990.

(2) Bryson, J. M.; Reineke, J. W.; Reineke, T. M. *Macromolecules* **2012**, *45*, 8939−8952.

(3) Xi, P. X.; Cheng, K.; Sun, X. L.; Zeng, Z. Z.; Sun, S. H. *Chem. Commun.* **2012**, *48*, 2952−2954.

(4) Zhang, F.; Braun, G. B.; Pallaoro, A.; Zhang, Y. C.; Shi, Y. F.; Cui, D. X.; Moskovits, M.; Zhao, D. Y.; Stucky, G. D. *Nano Lett.* **2012**, *12*, 61−67.

(5) Zhang, L.; Wang, Y. S.; Yang, Y.; Zhang, F.; Dong, W. F.; Zhou, S. Y.; Pei, W. H.; Chen, H. D.; Sun, H. B. *Chem. Commun.* **2012**, *48*, 11238−11240.

(6) Cheng, L.; Yang, K.; Li, Y. G.; Chen, J. H.; Wang, C.; Shao, M. W.; Lee, S. T.; Liu, Z. *Angew. Chem., Int. Ed.* **2011**, *50*, 7385−7390.

(7) Xu, H.; Cheng, L.; Wang, C.; Ma, X. X.; Li, Y. G.; Liu, Z. *Biomaterials* **2011**, *32*, 9364−9373.

(8) Yang, K.; Hu, L. L.; Ma, X. X.; Ye, S. Q.; Cheng, L.; Shi, X. Z.; Li, C. H.; Li, Y. G.; Liu, Z. *Adv. Mater.* **2012**, *24*, 1868−1872.
(9) Dong, W. J.; Li, Y. S.; Niu, D. C.; Ma, Z.; Liu, X. H.; Gu, J. L.; Zhao, W. R.; Zheng, Y. Y.; Shi, J. L. *Small* **2013**, *9*, 2500−2508, DOI: 10.1002/smll.201202649.
(10) Corr, S. A.; Rakovich, Y. P.; Gun'ko, Y. K. *Nanoscale Res. Lett.* **2008**, *3*, 87−104.
(11) Choi, J.; Kim, J. C.; Lee, Y. B.; Kim, I. S.; Park, Y. K.; Hur, N. H. *Chem. Commun.* **2007**, *23*, 1644−1646.
(12) Xu, S.; Song, X. J.; Guo, J.; Wang, C. C. *ACS Appl. Mater. Interfaces* **2012**, *4*, 4764−4775.
(13) Kim, J.; Lee, J. E.; Lee, J.; Yu, J. H.; Kim, B. C.; An, K.; Hwang, Y.; Shin, C. H.; Park, J. G.; Kim, J.; Hyeon, T. *J. Am. Chem. Soc.* **2006**, *128*, 688−689.
(14) Khatun, Z.; Nurunnabi, M.; Cho, K. J.; Lee, Y. K. *ACS Appl. Mater. Interfaces* **2012**, *4*, 3880−3887.
(15) Singh, N.; Charan, S.; Sanjiv, K.; Huang, S. H.; Hsiao, Y. C.; Kuo, C. W.; Chien, F. C.; Lee, T. C.; Chen, P. L. *Bioconjugate Chem.* **2012**, *23*, 421−430.
(16) Gu, Y. P.; Cui, R.; Zhang, Z. L.; Xie, Z. X.; Pang, D. W. *J. Am. Chem. Soc.* **2012**, *134*, 79−82.
(17) Chan, Y. H.; Ye, F. M.; Gallina, M. E.; Zhang, X. J.; Jin, Y. H.; Wu, I. C.; Chiu, D. T. *J. Am. Chem. Soc.* **2012**, *134*, 7309−7312.
(18) Harrison, B. S.; Foley, T. J.; Knefely, A. S.; Mwaura, J. K.; Cunningham, G. B.; Kang, T. S.; Bouguettaya, M.; Boncella, J. M.; Reynolds, J. R.; Schanze, K. S. *Chem. Mater.* **2004**, *16*, 2938−2947.
(19) Maity, S.; Sarkar, S.; Jana, P.; Maity, S. K.; Bera, S.; Mahalingam, V.; Haldar, D. *Soft Matter* **2012**, *8*, 7960−7966.
(20) Cheng, L.; Yang, K.; Zhang, S.; Shao, M. W.; Lee, S. T.; Liu, Z. *Nano Res.* **2010**, *3*, 722−732.
(21) Wang, C.; Tao, H. Q.; Cheng, L.; Liu, Z. *Biomaterials* **2011**, *32*, 6145−6154.
(22) Wang, C.; Cheng, L.; Liu, Z. *Biomaterials* **2011**, *32*, 1110−1120.
(23) Yang, L.; Li, X.; Yang, J. B.; Qu, Y.; Hua, J. L. *ACS Appl. Mater. Interfaces* **2013**, *5*, 1317−1326.
(24) Ahn, H. Y.; Yao, S.; Wang, X. H.; Belfield, K. D. *ACS Appl. Mater. Interfaces* **2012**, *4*, 2847−2854.
(25) Huber, J.; Jung, C.; Mecking, S. *Macromolecules* **2012**, *45*, 7799−7805.
(26) Yuan, L.; Lin, W. Y.; Yang, Y. T.; Chen, H. *J. Am. Chem. Soc.* **2012**, *134*, 1200−1211.
(27) Yuan, L.; Lin, W. Y.; Zhao, S.; Gao, W. S.; Chen, B.; He, L. W.; Zhu, S. S. *J. Am. Chem. Soc.* **2012**, *134*, 13510−13523.
(28) Karton-Lifshin, N.; Segal, E.; Omer, L.; Portnoy, M.; Satchi-Fainaro, R.; Shabat, D. *J. Am. Chem. Soc.* **2011**, *133*, 10960−10965.
(29) Yue, W.; Gao, J.; Li, Y.; Jiang, W.; Motta, S. D.; Negri, F.; Wang, Z. H. *J. Am. Chem. Soc.* **2011**, *133*, 18054−18057.
(30) Josephson, L.; Kircher, M. F.; Mahmood, U.; Tang, Y.; Weissleder, R. *Bioconjugate Chem.* **2002**, *13*, 554−560.
(31) Xie, J.; Chen, K.; Huang, J.; Lee, S.; Wang, J. H.; Gao, J. H.; Li, X. G.; Chen, X. Y. *Biomaterials* **2010**, *31*, 3016−3022.
(32) Tropiano, M.; Kilah, N. L.; Morten, M.; Rahman, H.; Davis, J. J.; Beer, P. D.; Faulkner, S. *J. Am. Chem. Soc.* **2011**, *133*, 11847−11849.
(33) Zhu, H.; Shang, Y. L.; Wang, W. H.; Zhou, Y. J.; Li, P. H.; Yan, K.; Wu, S. L.; Yeung, K. W. K.; Xu, Z. S.; Xu, P. H. B.; Chu, K. *Small* **2013**, *9*, 2991−3000, DOI: 10.1002/smll.201300126.
(34) Jin, T.; Yoshioka, Y.; Fujii, F.; Komai, Y.; Seki, J.; Seiyama, A. *Chem. Commun.* **2008**, *0*, 5764−5766.
(35) Park, J. H.; Maltzahn, G. V.; Ruoslahti, E.; Bhatia, S. N.; Sailor, M. J. *Angew. Chem., Int. Ed.* **2008**, *47*, 7284−7288.
(36) Wang, W.; Zhang, Y.; Yang, Q. B.; Sun, M. D.; Fei, X. L.; Song, Y.; Zhang, Y. M.; Li, Y. X. *Nanoscale* **2013**, *5*, 4958−4965.
(37) Li, J. G.; Jiang, H.; Yu, Z. Q.; Xia, H. Y.; Zou, G.; Zhang, Q. J.; Yu, Y. *Chem. Asian J.* **2013**, *8*, 385−391.
(38) Josephson, L.; Kircher, M. F.; Mahmood, U.; Tang, Y.; Weissleder, R. *Bioconjugate Chem.* **2002**, *13*, 554−560.
(39) Huang, P.; Li, Z. M.; Lin, J.; Yang, D. P.; Gao, G.; Xu, C.; Bao, L.; Zhang, C. L.; Wang, K.; Song, H.; Hu, H. Y.; Cui, D. X. *Biomaterials* **2011**, *32*, 3447−3458.
(40) Wu, W.; He, Q.; Jiang, C. Z. *Nanoscale Res. Lett.* **2008**, *3*, 397−415.
(41) Chang, Y. L.; Li, Y. P.; Meng, X. L.; Liu, N.; Sun, D. X.; Liu, H.; Wang, J. Y. *Polym. Chem.* **2013**, *4*, 789−794.
(42) Chen, K.; Xie, J.; Xu, H. Y.; Behera, D.; Michalski, M. H.; Biswal, S.; Wang, A.; Chen, X. Y. *Biomaterials* **2009**, *30*, 6912−6919.
(43) Jarzyna, P. A.; Skajaa, T.; Gianella, A.; Cormode, D. P.; Samber, D. D.; Dickson, S. D.; Chen, W.; Griffioen, A. W.; Fayad, Z. A.; Mulder, W. J. M. *Biomaterials* **2009**, *30*, 6947−6954.
(44) Lee, C. M.; Jang, D.; Kim, J.; Cheong, S. J.; Kim, E. M.; Jeong, M. H.; Kim, S. H.; Kim, D. W.; Lim, S. T.; Sohn, M. H.; Jeong, Y. Y.; Jeong, H. J. *Bioconjugate Chem.* **2011**, *22*, 186−192.
(45) Zhu, Y.; Tang, G. P.; Xu, F. J. *ACS Appl. Mater. Interfaces* **2013**, *5*, 1840−1848.
(46) Guo, W. H.; Zhu, J.; Cheng, Z. P.; Zhang, Z. B.; Zhu, X. L. *ACS Appl. Mater. Interfaces* **2011**, *3*, 1675−1680.
(47) Bai, L. J.; Zhang, L. F.; Pan, J. L.; Zhu, J.; Cheng, Z. P.; Zhu, X. L. *Macromolecules* **2013**, *46*, 2060−2066.
(48) Pan, J. L.; Zhang, L. F.; Bai, L. J.; Zhang, Z. B.; Chen, H.; Cheng, Z. P.; Zhu, X. L. *Polym. Chem.* **2013**, *4*, 2876−2883.
(49) Tsarevsky, N. V.; Matyjaszewski, K. *Chem. Rev.* **2007**, *107*, 2270−2299.
(50) Ouchi, M.; Terashima, T.; Sawamoto, M. *Chem. Rev.* **2009**, *109*, 4963−5050.
(51) Liu, J. L.; He, W. W.; Zhang, L. F.; Zhang, Z. B.; Zhu, J.; Yuan, L.; Chen, H.; Cheng, Z. P.; Zhu, X. L. *Langmuir* **2011**, *27*, 12684−12692.
(52) Xu, F. J.; Neoh, K. G.; Kang, E. T. *Prog. Polym. Sci.* **2009**, *34*, 719−761.
(53) Bai, L. J.; Zhang, L. F.; Cheng, Z. P.; Zhu, X. L. *Polym. Chem.* **2012**, *3*, 2685−2697.
(54) He, W. W.; Jiang, H. J.; Zhang, L. F.; Cheng, Z. P.; Zhu, X. L. *Polym. Chem.* **2013**, *4*, 2919−2938.
(55) Sun, S. H.; Zeng, H.; Robinson, D. B.; Raoux, S.; Rice, P. M.; Wang, S. X.; Li, G. X. *J. Am. Chem. Soc.* **2004**, *126*, 273−279.
(56) Vogt, C.; Toprak, M. S.; Muhammed, M.; Laurent, S.; Bridot, J. L.; Müller, R. N. *J. Nanopart. Res.* **2010**, *12*, 1137−1147.